



Cite this: *Phys. Chem. Chem. Phys.*, 2022, 24, 16484

# Aerosol mass spectrometry of neutral species based on a tunable vacuum ultraviolet free electron laser†

Xiangyu Zang,<sup>abc</sup> Zhaoyan Zhang,<sup>ab</sup> Shukang Jiang,<sup>a</sup> Yingqi Zhao,<sup>ab</sup> Tiantong Wang,<sup>ab</sup> Chong Wang,<sup>ab</sup> Gang Li,<sup>id a</sup> Hua Xie,<sup>id a</sup> Jiayue Yang,<sup>a</sup> Guorong Wu,<sup>id a</sup> Weiqing Zhang,<sup>a</sup> Jinian Shu,<sup>d</sup> Hongjun Fan,<sup>id \*a</sup> Xueming Yang<sup>id abce</sup> and Ling Jiang<sup>id \*a</sup>

A vacuum ultraviolet free electron laser (VUV-FEL) photoionization aerosol mass spectrometer (AMS) has been developed for online measurement of neutral compounds in laboratory environments. The aerosol apparatus is mainly composed of a smog chamber and a reflectron time-of-flight mass spectrometer (TOF-MS). The indoor smog chamber had a 2 m<sup>3</sup> fluorinated ethylene propylene film reactor placed in a temperature- and humidity-controlled room, which was used to generate the aerosols. The aerosols were sampled via an inlet system consisting of a 100 μm orifice nozzle and aerodynamic lenses. The application of this VUV-FEL AMS to the α-pinene ozonolysis under different concentrations reveals two new compounds, for which the formation mechanisms are proposed. The present findings contribute to the mechanistic understanding of the α-pinene ozonolysis in the neighborhood of emission origins of α-pinene. The VUV-FEL AMS method has the potential for chemical analysis of neutral aerosol species during the new particle formation processes.

Received 14th April 2022,  
Accepted 25th June 2022

DOI: 10.1039/d2cp01733d

rs.c.li/pccp

## 1. Introduction

Atmospheric pollution is becoming a severe issue in the developing world as it causes severe health and traffic problems for human society.<sup>1</sup> The formation of molecular compounds and their growth to larger sizes are critical to the nucleation of atmospheric aerosol particles, which have important influence on climate through indirect radiative effects.<sup>2–4</sup> Precise measurement of chemical compositions of molecular compounds and their dynamical changes with environmental conditions is a prerequisite for understanding the initial steps of atmospheric

aerosol formation. The key steps of atmospheric aerosol formation occur in the size range below 2 nm, in which direct detection of sub-2 nm aerosol species and their precursors has been proven to be a challenging experimental target.<sup>3</sup>

Aerosol mass spectrometry (AMS) is an essential method for real-time measurements of aerosols in both field and laboratory studies.<sup>5–31</sup> Numerous efforts have been devoted to the mass spectrometric study of charged species, for which the detection is easy. In contrast, neutral species present major experimental challenges because the absence of charge makes the detection difficult. Various techniques were utilized to ionize neutral aerosol species, such as chemical ionization, 70 eV electron impact, ultraviolet (UV), and vacuum ultraviolet (VUV) lasers.<sup>6–12,14,17,18,20,22–25,28,29,31</sup> Along with significant advances in theoretical calculations, these studies provided great insights into the sizes, structures, chemical compositions, and other characteristics of charged and neutral aerosols.

Recently, a Dalian Coherent Light Source (DCLS) facility has been developed,<sup>32</sup> which delivers a VUV free electron laser (VUV-FEL) with a continuously tunable wavelength in the 50–150 nm (8.3–24.8 eV) range. We have set up an infrared spectroscopic apparatus with this VUV-FEL, which allows for highly sensitive and size-selective photoionization of neutral clusters.<sup>33–38</sup> With this new technique, we find noncyclic three-dimensional structure of water clusters begins to exist already at

<sup>a</sup> State Key Laboratory of Molecular Reaction Dynamics, Dalian Institute of Chemical Physics, Chinese Academy of Sciences, 457 Zhongshan Road, Dalian 116023, China. E-mail: [ljjiang@dicp.ac.cn](mailto:ljjiang@dicp.ac.cn), [fanhj@dicp.ac.cn](mailto:fanhj@dicp.ac.cn)

<sup>b</sup> University of Chinese Academy of Sciences, 19A Yuquan Road, Beijing 100049, China

<sup>c</sup> Zhang Dayu School of Chemistry, Dalian University of Technology, 2 Linggong Road, Dalian 116024, China

<sup>d</sup> National Engineering Laboratory for VOCs Pollution Control Materials & Technology, University of Chinese Academy of Sciences, 380 Huaibei Village, Huairou District, Beijing 101408, China

<sup>e</sup> Department of Chemistry, School of Science, Southern University of Science and Technology, 1088 Xueyuan Avenue, Shenzhen 518055, China

† Electronic supplementary information (ESI) available: Detailed experimental methods and figures of the construction and characterization of smog chamber. See DOI: <https://doi.org/10.1039/d2cp01733d>

the pentamer with low finite temperature.<sup>35</sup> With trimethylamine–water as archetypical model bound by a single hydrogen bond, we have been able to resolve the previously masked coupling between the fluctuation of the hydrogen bond and the stretch of hydrogen-bonded OH.<sup>37</sup> In this work, we report the construction of an aerosol apparatus of VUV-FEL photoionization AMS (VUV-FEL AMS) and its preliminary applications to the standard organic compound and the  $\alpha$ -pinene ozonolysis.

## 2. Experimental method

Fig. 1 shows the schematic diagram of home-built aerosol apparatus, which is mainly composed of a smog chamber and a reflectron time-of-flight mass spectrometer (TOF-MS). Both the source (with aerodynamic lens assembly) and TOF-MS chambers were pumped using turbomolecular pumps (Edwards, STPA1603C) with a dinitrogen pumping speed of  $1600 \text{ L s}^{-1}$ . The differential chamber between the source and TOF-MS chambers was pumped by a turbomolecular pump (Edwards, STP301) with a dinitrogen pumping speed of  $300 \text{ L s}^{-1}$ . Note that one of us has constructed an aerosol apparatus coupled to the Advanced Light Source (ALS) at Lawrence Berkeley National Laboratory, which has multiple capabilities (*i.e.*, VUV light scattering, photoelectron imaging, and mass spectroscopy).<sup>15</sup> The different aspects of the present apparatus with respect to the previous one are described here.

### 2.1 Construction and characterization of smog chamber

The smog chamber was established at the Dalian Institute of Chemical Physics, Chinese Academy Sciences (hereafter referred as the “DICP-CAS chamber”), which had a volume of  $2 \text{ m}^3$  made of fluorinated ethylene propylene film (see ESI† for details).  $\text{O}_3$  was produced by an ozone generator (BNP Ozone technology Co., Model OZ-3G). The air dryer (Atlas Copco, Model F11) was used to get rid of water. The concentrations of  $\text{NO}/\text{NO}_2/\text{NO}_x$ ,  $\text{SO}_2$ , and  $\text{O}_3$  inside the reactor were measured by Thermo Scientific Model 42i, 43i, and 49i analyzers, respectively, and VOCs by proton-transfer reaction mass spectrometer (PTR-QMS 3000, East & West Analytical Instruments, China). Particle number concentrations and size distributions were

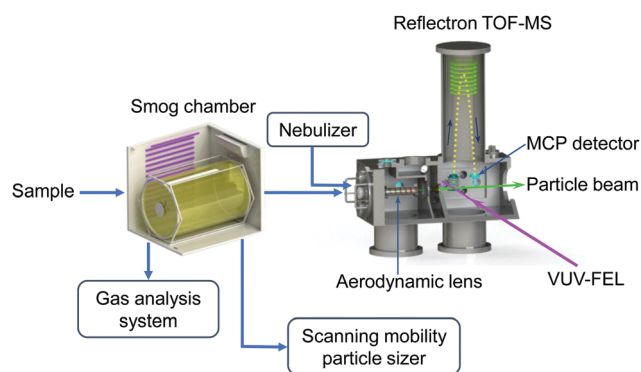


Fig. 1 Schematic view of aerosol apparatus based on a vacuum ultraviolet free electron laser.

Table 1 Comparison of wall loss rates of DICP-CAS chamber with other chamber facilities

Chamber name	Reactor volume ( $\text{m}^3$ )	Wall loss rates ( $\text{min}^{-1}$ )		
		NO	$\text{NO}_2$	$\text{O}_3$
GIG-CAS <sup>39</sup>	30	$1.41 \times 10^{-4}$	$1.39 \times 10^{-4}$	$1.31 \times 10^{-4}$
NCAT <sup>40</sup>	9	$7.40 \times 10^{-4}$	$3.47 \times 10^{-4}$	$5.90 \times 10^{-4}$
KNU <sup>41</sup>	7	$3.78 \times 10^{-4}$	$4.48 \times 10^{-5}$	$6.47 \times 10^{-5}$
Tsinghua <sup>42</sup>	2	$3.83 \times 10^{-5}$	$4.17 \times 10^{-5}$	$6.07 \times 10^{-4}$
DICP-CAS	2	$4.09 \times 10^{-4}$	$4.06 \times 10^{-4}$	$7.42 \times 10^{-4}$

measured by a scanning mobility particle sizer spectrometer (SMPS 3938NL76; TSI Incorporated, USA). The characterization results of the DICP-CAS chamber were shown in Fig. S1–S7 in ESI†, respectively. The wall loss rates of  $\text{NO}$ ,  $\text{NO}_2$ , and  $\text{O}_3$  are  $4.09 \times 10^{-4}$ ,  $4.06 \times 10^{-4}$ , and  $7.42 \times 10^{-4} \text{ min}^{-1}$ , respectively, which are all within the range of other chamber facilities (Table 1).

The particle size distribution during the dark  $\alpha$ -pinene ozonolysis as a function of time is shown in Fig. 2. With the injection of  $\text{O}_3$ , the  $\alpha$ -pinene ozonolysis happens rapidly and results in the formation of secondary organic aerosol (SOA). The SOA yield data obtained in the DICP-CAS chamber are consistent with other chamber facilities (Fig. S7, ESI†).

### 2.2 Reflectron TOF-MS

A silicone tube (inside diameter size: 6.35 mm; length: 1 m) was utilized to connect the reaction chamber and the MS chamber coupled to the VUV-FEL beamline. The sampling flow was about  $0.1 \text{ L min}^{-1}$ . The full aerosol population was transported by an aerodynamic lens assembly from the reaction chamber into the MS chamber. The aerodynamic lens assembly was similar to the “nanolenses” reported previously.<sup>43</sup> A nozzle of  $100 \mu\text{m}$  orifice was used to limit the aerosol flowrate into the aerodynamic lens system. An aperture with a 4 mm diameter was used to connect the source chamber and the differential chamber of the MS, while an aperture with a 3 mm diameter was used to connect the differential chamber and the TOF-MS detection chamber. The distance between the exit of aerodynamic lens assembly and the center of the photoionization

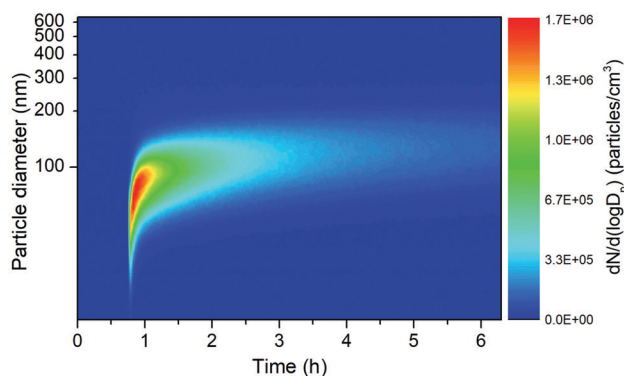


Fig. 2 Temporal evolution of the particle size distribution during the dark  $\alpha$ -pinene ozonolysis. The initial conditions are as follows:  $\alpha$ -pinene (92 ppb),  $\text{O}_3$  (584 ppb), 295 K, relative humidity 2.6%, all blacklights off.

region was 140 mm. For the present experiments, the compounds were continuously introduced into the center of the photoionization region of the TOF-MS.

The design of reflectron TOF-MS was a variant of the Wiley-McLaren type.<sup>44</sup> The extraction plates were powered by a high-voltage direct current (DC) of 2950 V, by which the charged compounds were deflected out of the particle beam by the DC electric field. The neutral compounds were ionized by VUV light in the center of the photoionization region of the TOF-MS. The electric fields of the drift tube and the reflector were shielded by a steel cylinder to avoid interfering with the flight of ions. The ions were detected using a dual microchannel plate (MCP). The transient signals from the MCP were first amplified by a fast preamplifier (FEMTO, DHPA-100) and then sent to a dual 1 GHz multiscaler (FAST ComTec GmbH, P7888-2) installed in a computer for real-time data collection. A delay generator (Stanford Research Systems, DG645) was utilized to control the timing sequence. The best resolution of VUV-FEL AMS is about  $M/\Delta M = 1800$  (Fig. S8, ESI<sup>†</sup>).

### 2.3 VUV laser system

The VUV-FEL light was generated at the DCLS described previously.<sup>33</sup> The VUV-FEL was operated in high-gain harmonic generation mode,<sup>45</sup> in which a seed laser was injected to interact with the electron beam in the modulator. Given the proper optimization of the linear accelerator, a high-quality beam with an emittance as low as  $\sim 1.5$  mm mrad, a projected energy spread of  $\sim 1\%$ , and a pulse duration of  $\sim 1.5$  ps can be obtained. The VUV-FEL pulse was currently operated at 20 Hz and can be tuned up to 50 Hz. The maximum pulse energy of the VUV-FEL was  $\sim 100$   $\mu$ J per pulse at 118 nm. An online VUV spectrometer was used to record the spectral characteristics (wavelength, energy, time profile) of every VUV-FEL pulse. In contrast with the tabletop four wave mixing (FWM) VUV laser, the VUV-FEL has two advantages, the wide range of tunable wavelength (50–150 nm) and the high pulse energy, which can be seen from Fig. 3 and 4 (*vide infra*). The pulse energy of the VUV-FEL ( $\sim 10^{14}$  photons per pulse) is about 6 orders higher than that of the ALS synchrotron VUV ( $\sim 10^8$  photons per pulse). However, the repetition rate of the VUV-FEL (10, 20, 25, and 50 Hz) is much lower than that of the ALS synchrotron VUV (quasicontinuous, 500 MHz). These capabilities of the VUV-FEL make it more suitable for the study of pulsed samples. Concerning that the high pulse energy may lead to saturation of photoionization, the VUV-FEL pulse energy dependence of the signal is routinely measured to ensure that the mass spectral intensity of a given species is linear with photon flux.

To compare with VUV-FEL photoionization efficiency, a tabletop FWM VUV light (118 nm) was generated by third harmonic generation (355 nm) of a Nd:YAG laser (Nimma-600) *via* Xe/Ar gas mixture at 1:10 relative concentration for 200 torr total pressure. The repetition rate and maximum pulse energy of FWM 118 nm light was 20 Hz and  $\sim 0.1$   $\mu$ J per pulse, respectively.

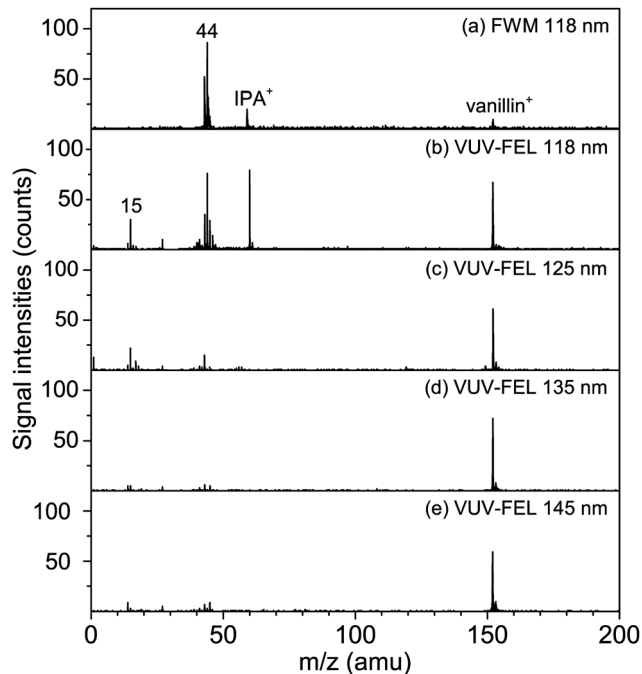


Fig. 3 Mass spectra of vanillin ionized by the tabletop FWM (118 nm) and the VUV-FEL (118 nm, 125 nm, 135 nm, and 145 nm). The peak labeled with “vanillin<sup>+</sup>” stands for molecular ion of the solute vanillin and “IPA<sup>+</sup>” for the solvent isopropanol (IPA), respectively.

## 3. Preliminary results

### 3.1 Comparison of mass spectra of organic compound ionized by the tabletop FWM and the VUV-FEL

The vanillin is taken as a model of organic compound for the comparison of FWM and VUV-FEL photoionization efficiency. The vanillin (>99%) was purchased from Aladdin. The isopropanol was used as the solvent. The concentration of the vanillin solution was 3.3 mmol L<sup>-1</sup>. The vanillin aerosols were generated with a traditional jet nebulizer by nebulizing the solutions (Fig. 1). The flow rate of the nebulization was 3.5 L min<sup>-1</sup>.

Fig. 3 shows the mass spectra of vanillin ionized by the FWM (118 nm) and the VUV-FEL (118 nm, 125 nm, 135 nm, and 145 nm). Note that the ionization energy of the vanillin is 8.31 eV (149.2 nm)<sup>46</sup> and that of the isopropanol is 10.15 eV (122.1 nm),<sup>47,48</sup> respectively. With the FWM (118 nm) photoionization (Fig. 3a), the molecular ion ( $m/z = 152$ , labeled with “vanillin<sup>+</sup>”) of vanillin (C<sub>8</sub>H<sub>8</sub>O<sub>3</sub>) is weakly observed,<sup>46,49</sup> while the molecular ion ( $m/z = 60$ , labeled with “IPA<sup>+</sup>”) of isopropanol (C<sub>3</sub>H<sub>8</sub>O, IPA) is readily detected as well as the  $m/z = 44$  signal.<sup>48,50,51</sup> Note that the VUV photon energy at 118 nm (10.51 eV) is about 2.20 eV higher than the ionization energy of vanillin (8.31 eV), the photoionization could be saturated for vanillin even with the FWM 118 nm light. With the VUV-FEL 118 nm photoionization of vanillin, the detector is found to be readily saturated with the intense signal and its detection threshold has to be reduced. Thus, the enhancement extent for the vanillin<sup>+</sup> signal intensity is not linearly dependent on the high pulse energy of VUV-FEL, resulting in the difficulty of

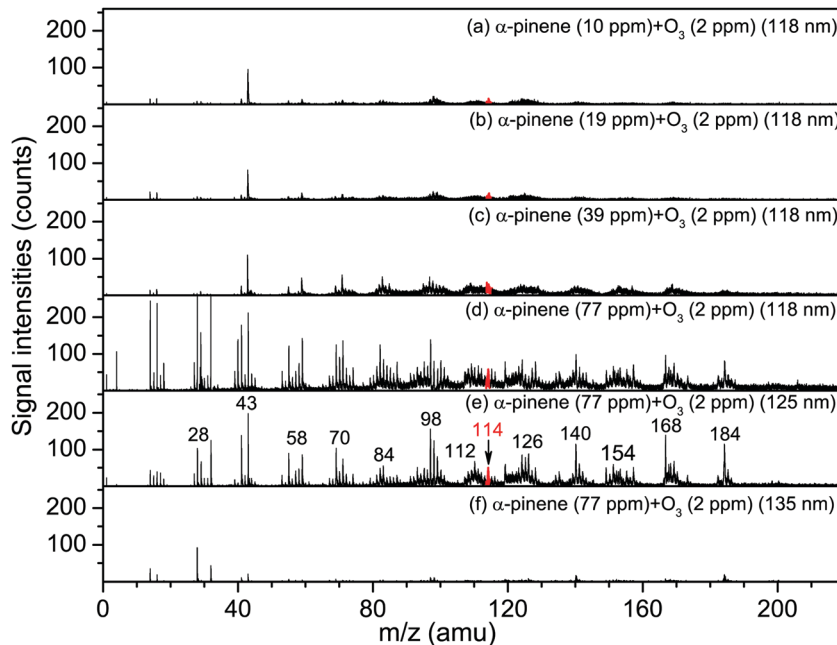


Fig. 4 VUV-FEL photoionization mass spectra of the compounds generated from the  $\alpha$ -pinene ozonolysis in the DICP-CAS chamber.

direct assessment of the increase magnitude of vanillin signal. While the wavelength and the pulse energy of VUV-FEL can be tuned, the saturation of VUV-FEL photoionization could be avoided.

When tuning the wavelength of VUV-FEL to 125 nm with the VUV photon energy lower than the ionization energy of IPA, the  $\text{IPA}^+$  ions disappear (Fig. 3c). In contrast with the VUV-FEL 118 nm mass spectrum, the intensities of the  $m/z = 15$  and 44 fragments are substantially reduced at 125 nm and become negligible at 135 nm and 145 nm, whereas the intensities of the vanillin<sup>+</sup> ions are virtually unchanged. Small amounts of the  $m/z = 15$  and 44 signals are also observed in the VUV-FEL 125 nm spectra where the photon energy is below the ionization threshold of IPA. This suggests that the contribution for the  $m/z = 15$  ( $\text{CH}_3^+$ ) and 44 ( $\text{CH}_2=\text{CHOH}^+$ ) fragments might be mainly from the massive solvent isopropanol and minorly from the solute vanillin, for which the fragmentation mechanisms have been previously discussed in detail.<sup>48,50,51</sup> These results demonstrate that the tunable VUV-FEL allows for photoionization of neutral compounds with high sensitivity and selectivity.

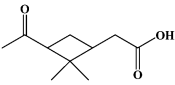
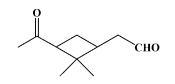
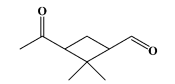
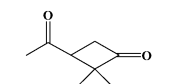
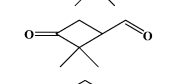
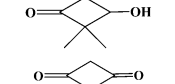

### 3.2 VUV-FEL photoionization mass spectra of $\alpha$ -pinene ozonolysis

The oxidation of volatile organic compounds (VOCs) is a major source of SOA, which is known to affect the Earth's radiation balance by scattering solar radiation and by acting as cloud condensation nuclei.<sup>52,53</sup> While monoterpene represents an important family of VOCs,  $\alpha$ -pinene is the most abundant monoterpene in the atmosphere and its oxidation has attracted considerable attention.<sup>54,55</sup> The reaction of  $\alpha$ -pinene with ozone has been studied using various experimental techniques, such as gas chromatography, electron-impact mass spectrometry, chemical-impact mass spectrometry, and Fourier transform infrared spectro-

scopy.<sup>56-63</sup> The major products of pinonaldehyde, nor-pinonic acid, and pinonic acid have been identified. Here, the  $\alpha$ -pinene ozonolysis is chosen as an example to demonstrate the capability of the VUV-FEL AMS method for online characterization of neutral compounds generated in the smog chamber. The  $\alpha$ -pinene (>99%) was purchased from Aladdin.

Fig. 4 shows the VUV-FEL photoionization mass spectra of the compounds generated from the  $\alpha$ -pinene ozonolysis under different concentrations, in which the size distribution for the products is  $\sim 100$  nm, similar to that shown in Fig. 2. The  $m/z = 126, 140, 154, 168,$  and  $184$  compounds are assigned on the basis of the previous studies,<sup>57</sup> and their identifications, molecular structures, and formula are listed in Table 2. The peaks below 90 Da, including those with  $m/z$  centered at 28, 43, 58, 70, and 84, could be attributed to the fragment ions of compounds bearing hydrocarbon, carboxyl, hydroxy, and ketone groups, similar to the results observed using atmospheric pressure ionization mass spectrometry<sup>64</sup> and thermal-desorption dichloromethane-induced low-pressure photoionization mass spectrometry.<sup>61</sup> In addition, two new peaks at  $m/z = 112$  and 114 are observed. As exemplified by the  $m/z = 114$  peak, mass spectral intensity increases with the increase of the concentration of  $\alpha$ -pinene (Fig. 5). Better mass spectral resolution is obtained at the 125 nm photoionization. As shown Fig. 4d and e, the intensities of the peaks below 90 Da in the 118 nm spectra are stronger than those in the 125 nm spectra, in the price of the reduced intensities of the  $m/z = 140, 168,$  and  $184$  peaks, indicating that the peaks below 90 Da could be ascribed to the fragments generated from the  $m/z = 140, 168,$  and  $184$  compounds. The intensities of the  $m/z = 112$  and 114 peaks do not remarkably vary in the 118 nm and 125 nm spectra, implying that the  $m/z = 112$  and 114 compounds are not fragments produced during ionization.

Table 2 Products identified in the reaction of  $\alpha$ -pinene with  $O_3$  in the smog chamber

Molecular weight	Identification	Structure	Formula
184	Pinonic acid		$C_{10}H_{16}O_3$
168	Pinonaldehyde		$C_{10}H_{16}O_2$
154	Norpinonaldehyde		$C_9H_{14}O_2$
140	3-Oxo-2,2-dimethylcyclobutyl-ethanone		$C_8H_{12}O_2$
126	3-Oxo-2,2-dimethyl-cyclobutyl-methanal		$C_7H_{10}O_2$
114	2,2-Dimethyl-3-hydroxyl-cyclobutanone		$C_6H_{10}O_2$
112	2,2-Dimethyl-1,3-cyclobutanedione		$C_6H_8O_2$

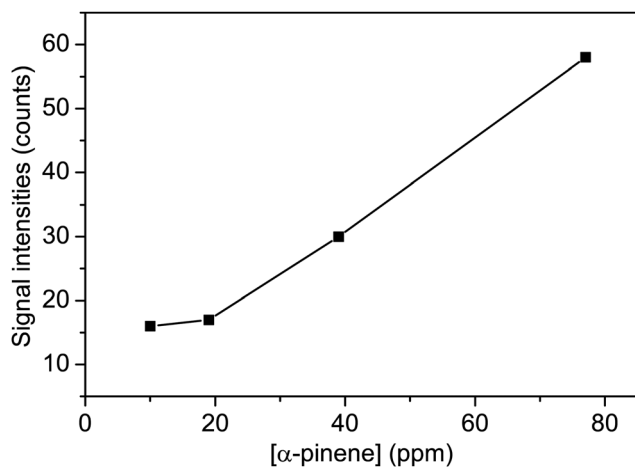


Fig. 5 The signal intensities of the  $m/z = 114$  peak as a function of the concentration of  $\alpha$ -pinene. The mass spectra were measured at the VUV-FEL 118 nm.

The influence of the addition of the OH radical scavenger (cyclohexane) on the  $\alpha$ -pinene ozonolysis was investigated. As shown in Fig. 6, the  $m/z = 112$  and  $114$  peaks are remarkably reduced to be negligible in the presence of the OH scavenger, indicating that the OH is involved in the formation of the  $m/z = 112$  and  $114$  compounds. No obvious peaks are observed in the VUV-FEL photoionization mass spectra of the compounds generated from the pure  $\alpha$ -pinene experiments (Fig. S9–S11, ESI<sup>†</sup>), suggesting that the impurity of  $\alpha$ -pinene sample or the autoxidation product of  $\alpha$ -pinene does not contribute to the formation of the  $m/z = 112$  and  $114$  compounds.

In order to understand the experimental mass spectra of  $\alpha$ -pinene ozonolysis, quantum chemical calculations were

carried out at the  $\omega$ B97XD/def2-TZVP level of theory using the Gaussian 09 program.<sup>65</sup> The formation mechanism of the  $m/z = 112$  and  $114$  compounds is proposed in Fig. 7. The  $1 \rightarrow 2$  reaction ( $O_3$  cycloaddition process) is predicted to be highly exothermic ( $61.6 \text{ kcal mol}^{-1}$ ) with a very small barrier ( $5.4 \text{ kcal mol}^{-1}$ ) (Fig. 7), which is consistent with the previous studies.<sup>62,66</sup> The  $2 \rightarrow 3$  reaction (C–C bond cleavage) is both thermodynamically exothermic and kinetically facile with a barrier of  $21.5 \text{ kcal mol}^{-1}$ . The  $3 \rightarrow 4$  reaction is intramolecular hydrogen abstraction of H(CH<sub>2</sub>) by terminal O atom, which is exothermic ( $21.7 \text{ kcal mol}^{-1}$ ) with a barrier of  $19.3 \text{ kcal mol}^{-1}$ . The  $4 \rightarrow 5$  reaction (C=C ozonolysis) is facile according to the  $1 \rightarrow 3$  reaction, which is highly exothermic by  $85.7 \text{ kcal mol}^{-1}$ . The isomerization from 5 to 5a is exothermic by  $23.1 \text{ kcal mol}^{-1}$  with a barrier of  $22.3 \text{ kcal mol}^{-1}$ , which is in accord with the observation of peroxy species.<sup>63</sup> The  $5a \rightarrow 6$  reaction is hydrogen abstraction by OH with the O–O bond cleavage, which is highly exothermic ( $100.1 \text{ kcal mol}^{-1}$ ). Note that the energy for the adduct of 5a and OH is lower than 5a by  $5.0 \text{ kcal mol}^{-1}$ , indicating that the barrier of the  $5a \rightarrow 6$  reaction is  $4.8 \text{ kcal mol}^{-1}$ . Compound 6 releases  $CO_2$  to produce 7, which is predicted to be exothermic by  $12.0 \text{ kcal mol}^{-1}$  with a very small barrier of  $2.2 \text{ kcal mol}^{-1}$ . Compound 7 reacts with  $O_2$  to generate 8, which is calculated to be exothermic by  $36.5 \text{ kcal mol}^{-1}$ .

Compound 8 donates O to the C=C bond of 1 with the formation of 9, which is exothermic by  $32.5 \text{ kcal mol}^{-1}$  with a barrier of  $5.8 \text{ kcal mol}^{-1}$ . 9 reacts with  $O_2$  to form 10, which is calculated to be exothermic by  $30.1 \text{ kcal mol}^{-1}$  with a barrier of  $12.1 \text{ kcal mol}^{-1}$ . The  $10 \rightarrow 11$  reaction is hydrogen abstraction by OH with the release of  $H_2O$ , which is predicted to be exothermic by  $24.9 \text{ kcal mol}^{-1}$  with a barrier of  $0.9 \text{ kcal mol}^{-1}$ . The  $11 \rightarrow 12$  reaction (C=C ozonolysis) is facile according to the  $1 \rightarrow 3$  reaction, which is highly

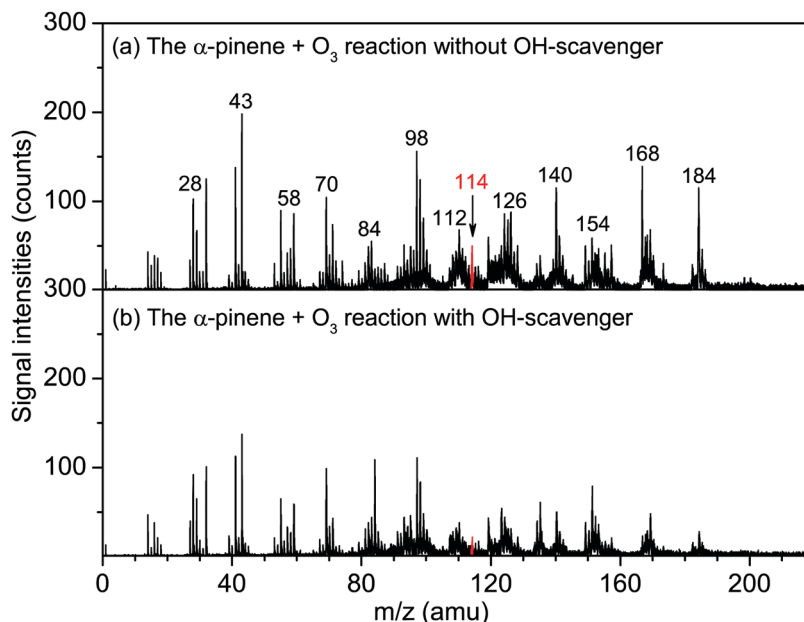


Fig. 6 VUV-FEL photoionization mass spectra of the compounds generated from the  $\alpha$ -pinene (77 ppm) +  $O_3$  (2 ppm) reaction without/with OH-scavenger. The compounds were ionized by the VUV-FEL at 125 nm.

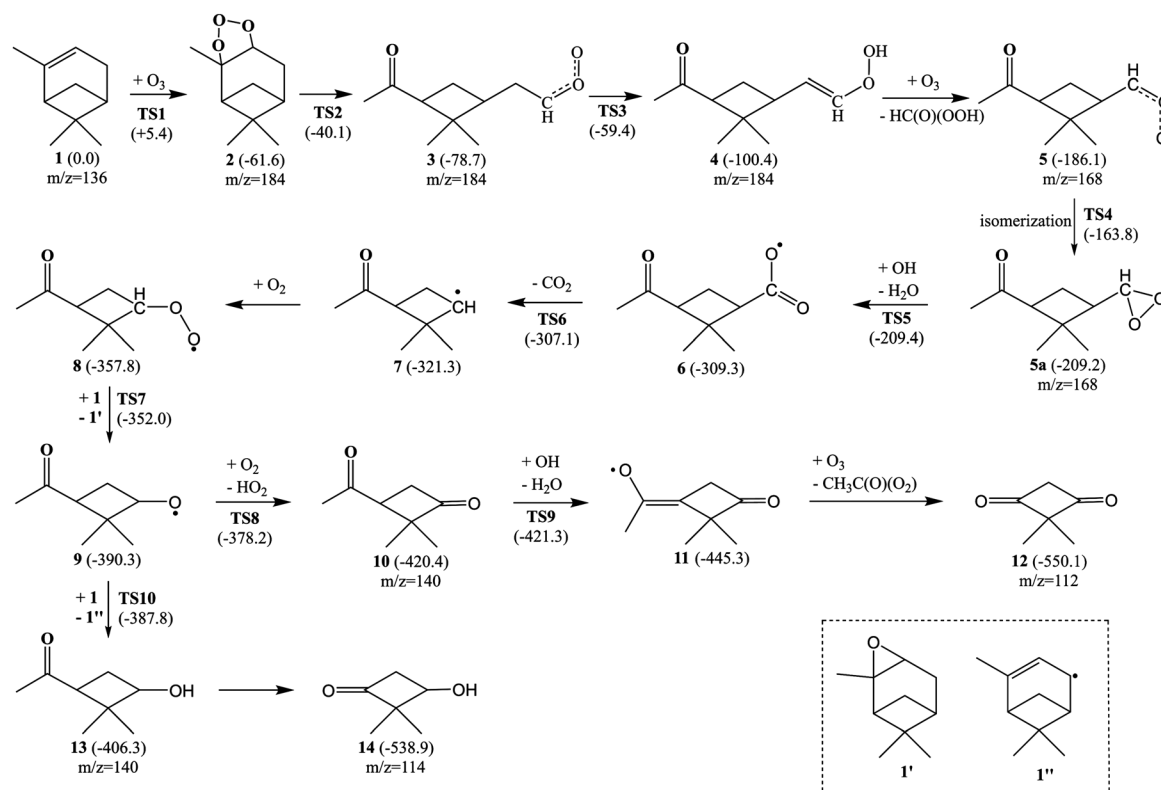


Fig. 7 Proposed formation mechanism of the  $m/z = 112$  and  $114$  compounds from the reaction of  $\alpha$ -pinene with  $O_3$ . Calculations were performed at the  $\omega$ B97XD/def2-TZVP level of theory. Energies are listed in  $\text{kcal mol}^{-1}$ , which are relative to  $\alpha$ -pinene. The structures of  $1'$  and  $1''$  are shown in the dashed-lined square.

exothermic by  $104.8 \text{ kcal mol}^{-1}$ . Compound **9** abstracts hydrogen from **1** to form **13**, which is predicted to be exothermic by  $16.0 \text{ kcal mol}^{-1}$  with a barrier of

$2.5 \text{ kcal mol}^{-1}$ . The **13**  $\rightarrow$  **14** reaction is facile according to the **10**  $\rightarrow$  **12** reaction, resulting in the formation of the  $m/z = 114$  compound.

It can be seen from Fig. 7 that the  $\alpha$ -pinene (**1**) is involved in the **8**  $\rightarrow$  **9** and **9**  $\rightarrow$  **13** reactions, suggesting that the higher concentration of  $\alpha$ -pinene is helpful for the generation of more amounts of compounds **12** and **14**. The proposed mechanism thus supports the experimental observation of compound **12** ( $m/z = 112$ ) and compound **14** ( $m/z = 114$ ) under high concentration of  $\alpha$ -pinene. These results would help to understand the complicated reaction mechanisms of the  $\alpha$ -pinene ozonolysis nearby the emission origins with concentrated  $\alpha$ -pinene.<sup>53–55,60,61,63</sup>

## 4. Conclusion

We report the construction and characterization of an aerosol mass spectrometer (AMS) of neutral compounds based on photoionization using a tunable vacuum ultraviolet free-electron laser (VUV-FEL AMS). The comparison of mass spectra of vanillin ionized by the VUV-FEL and the tabletop four wave mixing VUV indicates the sensitivity and selectivity of VUV-FEL photoionization. The VUV-FEL photoionization mass spectra of the  $\alpha$ -pinene ozonolysis under high concentration of  $\alpha$ -pinene reveal two new compounds. The present findings contribute to the mechanistic understanding of the complicated reactions of the  $\alpha$ -pinene ozonolysis nearby the original circumstances of the emission of concentrated  $\alpha$ -pinene. The VUV-FEL AMS method presents a promising paradigm for the study of a wide variety of neutral aerosol species.

## Author contributions

L. J. and H. F. designed the research. X. Z., S. J., Y. Z., T. W., C. W., G. L., H. X., J. Y., W. Z., G. W., J. S., X. Y., and L. J. performed the experiments and data analysis; Z. Z. and H. F. performed the theoretical calculations and data analysis; L. J. and H. F. cowrote the manuscript.

## Conflicts of interest

The authors declare no competing financial interest.

## Acknowledgements

The authors gratefully acknowledge the Dalian Coherent Light Source (DCLS) for support and assistance. This work was financially supported by the National Natural Science Foundation of China (22125303, 92061203, 92061114 and 22288201), the Strategic Priority Research Program of the Chinese Academy of Sciences (CAS) (XDB17000000), and Dalian Institute of Chemical Physics (DICP DCLS201702).

## References

- 1 E. von Schneidemesser, P. S. Monks, J. D. Allan, L. Bruhwiler, P. Förster, D. Fowler, A. Lauer, W. T. Morgan, P. Paasonen,

- M. Righi, K. Sindelarova and M. A. Sutton, *Chem. Rev.*, 2015, **115**, 3856–3897.
- 2 R. Zhang, A. Khalizov, L. Wang, M. Hu and W. Xu, *Chem. Rev.*, 2012, **112**, 1957–2011.
- 3 M. Kulmala, J. Kontkanen, H. Junninen, K. Lehtipalo, H. E. Manninen, T. Nieminen, T. Petaja, M. Sipila, S. Schobesberger, P. Rantala, A. Franchin, T. Jokinen, E. Jarvinen, M. Aijala, J. Kangasluoma, J. Hakala, P. P. Aalto, P. Paasonen, J. Mikkila, J. Vanhanen, J. Aalto, H. Hakola, U. Makkonen, T. Ruuskanen, R. L. Mauldin, III, J. Duplissy, H. Vehkamäki, J. Back, A. Kortelainen, I. Riipinen, T. Kurten, M. V. Johnston, J. N. Smith, M. Ehn, T. F. Mentel, K. E. J. Lehtinen, A. Laaksonen, V.-M. Kerminen and D. R. Worsnop, *Science*, 2013, **339**, 943–946.
- 4 L. Yao, O. Garmash, F. Bianchi, J. Zheng, C. Yan, J. Kontkanen, H. Junninen, S. B. Mazon, M. Ehn, P. Paasonen, M. Sipila, M. Wang, X. Wang, S. Xiao, H. Chen, Y. Lu, B. Zhang, D. Wang, Q. Fu, F. Geng, L. Li, H. Wang, L. Qiao, X. Yang, J. Chen, V.-M. Kerminen, T. Petaja, D. R. Worsnop, M. Kulmala and L. Wang, *Science*, 2018, **361**, 278–281.
- 5 E. Woods, G. D. Smith, Y. Dessiaterik, T. Baer and R. E. Miller, *Anal. Chem.*, 2001, **73**, 2317–2322.
- 6 E. Woods, G. D. Smith, R. E. Miller and T. Baer, *Anal. Chem.*, 2002, **74**, 1642–1649.
- 7 D. C. Sykes, E. Woods, G. D. Smith, T. Baer and R. E. Miller, *Anal. Chem.*, 2002, **74**, 2048–2052.
- 8 J. L. Jimenez, J. T. Jayne, Q. Shi, C. E. Kolb, D. R. Worsnop, I. Yourshaw, J. H. Seinfeld, R. C. Flagan, X. F. Zhang, K. A. Smith, J. W. Morris and P. Davidovits, *J. Geophys. Res.: Atmos.*, 2003, **108**, 8425.
- 9 D. Voisin, J. N. Smith, H. Sakurai, P. H. McMurry and F. L. Eisele, *Aerosol Sci. Technol.*, 2003, **37**, 471–475.
- 10 B. Oktem, M. P. Tolocka and M. V. Johnston, *Anal. Chem.*, 2004, **76**, 253–261.
- 11 J. N. Smith, K. F. Moore, P. H. McMurry and F. L. Eisele, *Aerosol Sci. Technol.*, 2004, **38**, 100–110.
- 12 P. J. Popp, R. S. Gao, T. P. Marcy, D. W. Fahey, P. K. Hudson, T. L. Thompson, B. Karcher, B. A. Ridley, A. J. Weinheimer, D. J. Knapp, D. D. Montzka, D. Baumgardner, T. J. Garrett, E. M. Weinstock, J. B. Smith, D. S. Sayres, J. V. Pittman, S. Dhaniala, T. P. Bui and M. J. Mahoney, *J. Geophys. Res.: Atmos.*, 2004, **109**, D06302.
- 13 R. C. Sullivan and K. A. Prather, *Anal. Chem.*, 2005, **77**, 3861–3885.
- 14 E. R. Mysak, K. R. Wilson, M. Jimenez-Cruz, M. Ahmed and T. Baer, *Anal. Chem.*, 2005, **77**, 5953–5960.
- 15 J. N. Shu, K. R. Wilson, M. Ahmed and S. R. Leone, *Rev. Sci. Instrum.*, 2006, **77**, 043106.
- 16 D. G. Nash, T. Baer and M. V. Johnston, *Int. J. Mass Spectrom.*, 2006, **258**, 2–12.
- 17 E. Gloaguen, E. R. Mysak, S. R. Leone, M. Ahmed and K. R. Wilson, *Int. J. Mass Spectrom.*, 2006, **258**, 74–85.
- 18 P. F. DeCarlo, J. R. Kimmel, A. Trimborn, M. J. Northway, J. T. Jayne, A. C. Aiken, M. Gonin, K. Fuhrer, T. Horvath,

- K. S. Docherty, D. R. Worsnop and J. L. Jimenez, *Anal. Chem.*, 2006, **78**, 8281–8289.
- 19 D. M. Murphy, *Mass Spectrom. Rev.*, 2007, **26**, 150–165.
- 20 M. J. Northway, J. T. Jayne, D. W. Toohey, M. R. Canagaratna, A. Trimborn, K. I. Akiyama, A. Shimono, J. L. Jimenez, P. F. DeCarlo, K. R. Wilson and D. R. Worsnop, *Aerosol Sci. Technol.*, 2007, **41**, 828–839.
- 21 T. Streibel, S. Mitschke, T. Adam, J. Weh and R. Zimmermann, *J. Anal. Appl. Pyrolysis*, 2007, **79**, 24–32.
- 22 M. R. Canagaratna, J. T. Jayne, J. L. Jimenez, J. D. Allan, M. R. Alfarra, Q. Zhang, T. B. Onasch, F. Drewnick, H. Coe, A. Middlebrook, A. Delia, L. R. Williams, A. M. Trimborn, M. J. Northway, P. F. DeCarlo, C. E. Kolb, P. Davidovits and D. R. Worsnop, *Mass Spectrom. Rev.*, 2007, **26**, 185–222.
- 23 J. Shu, S. Gao and Y. Li, *Aerosol Sci. Technol.*, 2008, **42**, 110–113.
- 24 A. Zelenyuka, J. Yang and D. Imre, *Int. J. Mass Spectrom.*, 2009, **282**, 6–12.
- 25 A. Zelenyuk, J. Yang, D. Imre and E. Choi, *Aerosol Sci. Technol.*, 2009, **43**, 305–310.
- 26 D. K. Farmer and J. L. Jimenez, *Anal. Chem.*, 2010, **82**, 7879–7884.
- 27 S. Geddes, B. Nichols, S. Flemer, Jr., J. Eisenhauer, J. Zahardis and G. A. Petrucci, *Anal. Chem.*, 2010, **82**, 7915–7923.
- 28 H. Junninen, M. Ehn, T. Petaja, L. Luosujarvi, T. Kotiaho, R. Kostiaainen, U. Rohner, M. Gonin, K. Fuhrer, M. Kulmala and D. R. Worsnop, *Atmos. Meas. Tech.*, 2010, **3**, 1039–1053.
- 29 W. Fang, L. Gong, X. Shan, F. Liu, Z. Wang and L. Sheng, *Anal. Chem.*, 2011, **83**, 9024–9032.
- 30 J. Zahardis, S. Geddes and G. A. Petrucci, *Anal. Chem.*, 2011, **83**, 2409–2415.
- 31 W. Q. Sun, J. N. Shu, P. Zhang, Z. Li, N. N. Li, M. Liang and B. Yang, *Atmos. Meas. Tech.*, 2015, **8**, 4637–4643.
- 32 D. Normile, *Science*, 2017, **355**, 235.
- 33 B. B. Zhang, Y. Yu, Z. J. Zhang, Y. Y. Zhang, S. K. Jiang, Q. M. Li, S. Yang, H. S. Hu, W. Q. Zhang, D. X. Dai, G. R. Wu, J. Li, D. H. Zhang, X. M. Yang and L. Jiang, *J. Phys. Chem. Lett.*, 2020, **11**, 851–855.
- 34 G. Li, C. Wang, Q. Li, H. Zheng, T. Wang, Y. Yu, M. Su, D. Yang, L. Shi, J. Yang, Z. He, H. Xie, H. Fan, W. Zhang, D. Dai, G. Wu, X. Yang and L. Jiang, *Rev. Sci. Instrum.*, 2020, **91**, 034103.
- 35 B. B. Zhang, Y. Yu, Y. Y. Zhang, S. K. Jiang, Q. M. Li, H. S. Hu, G. Li, Z. Zhao, C. Wang, H. Xie, W. Q. Zhang, D. X. Dai, G. R. Wu, D. H. Zhang, L. Jiang, J. Li and X. M. Yang, *Proc. Natl. Acad. Sci. U. S. A.*, 2020, **117**, 15423–15428.
- 36 G. Li, Y. Y. Zhang, Q. M. Li, C. Wang, Y. Yu, B. B. Zhang, H. S. Hu, W. Q. Zhang, D. X. Dai, G. R. Wu, D. H. Zhang, J. Li, X. M. Yang and L. Jiang, *Nat. Commun.*, 2020, **11**, 5449.
- 37 S. Jiang, M. Su, S. Yang, C. Wang, Q.-R. Huang, G. Li, H. Xie, J. Yang, G. Wu, W. Zhang, Z. Zhang, J.-L. Kuo, Z.-F. Liu, D. H. Zhang, X. Yang and L. Jiang, *J. Phys. Chem. Lett.*, 2021, **12**, 2259–2265.
- 38 C. Wang, Q. M. Li, X. T. Kong, H. J. Zheng, T. T. Wang, Y. Zhao, G. Li, H. Xie, J. Y. Yang, G. R. Wu, W. Q. Zhang, D. X. Dai, M. F. Zhou, X. M. Yang and L. Jiang, *J. Phys. Chem. Lett.*, 2021, **12**, 1012–1017.
- 39 X. Wang, T. Liu, F. Bernard, X. Ding, S. Wen, Y. Zhang, Z. Zhang, Q. He, S. Lu, J. Chen, S. Saunders and J. Yu, *Atmos. Meas. Tech.*, 2014, **7**, 301–313.
- 40 D. M. Smith, M. N. Fiddler, K. G. Sexton and S. Bililign, *Aerosol Air Qual. Res.*, 2019, **19**, 467–483.
- 41 Z. Bin Babar, J.-H. Park, J. Kang and H.-J. Lim, *Aerosol Air Qual. Res.*, 2016, **16**, 3102–3113.
- 42 S. Wu, Z. Lu, J. Hao, Z. Zhao, J. Li, H. Takekawa, H. Minoura and A. Yasuda, *Adv. Atmos. Sci.*, 2007, **24**, 250–258.
- 43 X. Wang and P. H. McMurry, *Int. J. Mass Spectrom.*, 2006, **258**, 30–36.
- 44 W. C. Wiley and I. H. McLaren, *Rev. Sci. Instrum.*, 1955, **26**, 1150–1157.
- 45 L. H. Yu, M. Babzien, I. Ben-Zvi, L. F. DiMauro, A. Doyuran, W. Graves, E. Johnson, S. Krinsky, R. Malone, I. Pogorelsky, J. Skaritka, G. Rakowsky, L. Solomon, X. J. Wang, M. Woodle, V. Yakimenko, S. G. Biedron, J. N. Galayda, E. Gluskin, J. Jagger, V. Sajaev and I. Vasserman, *Science*, 2000, **289**, 932–934.
- 46 X. Wu, X. Zhou, S. Bjelic, P. Hemberger and A. Bodi, *J. Phys. Chem. A*, 2021, **125**, 3327–3340.
- 47 K. Watanabe, *J. Chem. Phys.*, 1957, **26**, 542–547.
- 48 K. M. A. Refaey and W. A. Chupka, *J. Chem. Phys.*, 1968, **48**, 5205–5219.
- 49 L. Tao, M. Huang, W. Zhang, Z. Wang, W. Fang, X. Shan, F. Liu and L. Sheng, *Acta Chim. Sin.*, 2010, **68**, 2059–2062.
- 50 L. Friedman, F. A. Long and M. Wolfsberg, *J. Chem. Phys.*, 1957, **27**, 613–622.
- 51 L.-X. Wei, B. Yang, J. Wang, C.-Q. Huang, L.-S. Sheng and F. Qi, *Acta Phys.-Chim. Sin.*, 2006, **22**, 987–992.
- 52 M. Ehn, J. A. Thornton, E. Kleist, M. Sipila, H. Junninen, I. Pullinen, M. Springer, F. Rubach, R. Tillmann, B. Lee, F. Lopez-Hilfiker, S. Andres, I.-H. Acir, M. Rissanen, T. Jokinen, S. Schobesberger, J. Kangasluoma, J. Kontkanen, T. Nieminen, T. Kurten, L. B. Nielsen, S. Jorgensen, H. G. Kjaergaard, M. Canagaratna, M. Dal Maso, T. Berndt, T. Petaja, A. Wahner, V.-M. Kerminen, M. Kulmala, D. R. Worsnop, J. Wildt and T. F. Mentel, *Nature*, 2014, **506**, 476–479.
- 53 B. Noziere, M. Kaberer, M. Claeys, J. Allan, B. D'Anna, S. Decesari, E. Finessi, M. Glasius, I. Grgic, J. F. Hamilton, T. Hoffmann, Y. Iinuma, M. Jaoui, A. Kahno, C. J. Kampf, I. Kourtchev, W. Maenhaut, N. Marsden, S. Saarikoski, J. Schnelle-Kreis, J. D. Surratt, S. Szidat, R. Szmigielski and A. Wisthaler, *Chem. Rev.*, 2015, **115**, 3919–3983.
- 54 A. Guenther, C. N. Hewitt, D. Erickson, R. Fall, C. Geron, T. Graedel, P. Harley, L. Klinger, M. Lerdau, W. A. McKay, T. Pierce, B. Scholes, R. Steinbrecher, R. Tallamraju, J. Taylor and P. Zimmerman, *J. Geophys. Res.: Atmos.*, 1995, **100**, 8873–8892.
- 55 R. J. Griffin, D. R. Cocker, J. H. Seinfeld and D. Dabdub, *Geophys. Res. Lett.*, 1999, **26**, 2721–2724.



- 56 M. Jang and R. M. Kamens, *Atmos. Environ.*, 1999, **33**, 459–474.
- 57 M. Jaoui and R. M. Kamens, *Atmos. Environ.*, 2003, **37**, 1835–1851.
- 58 Y. Iinuma, O. Boge, T. Gnauk and H. Herrmann, *Atmos. Environ.*, 2004, **38**, 761–773.
- 59 Y. Yu, M. J. Ezell, A. Zelenyuk, D. Imre, L. Alexander, J. Ortega, B. D'Anna, C. W. Harmon, S. N. Johnson and B. J. Finlayson-Pitts, *Atmos. Environ.*, 2008, **42**, 5044–5060.
- 60 X. Zhang, R. C. McVay, D. D. Huang, N. F. Dalleska, B. Aumont, R. C. Flagan and J. H. Seinfeld, *Proc. Natl. Acad. Sci. U. S. A.*, 2015, **112**, 14168–14173.
- 61 P. Zhang, P. Ma, J. Shu, J. Huang, B. Yang and H. Zhang, *Atmos. Environ.*, 2019, **213**, 47–54.
- 62 A. Bagchi, Y. Yu, J.-H. Huang, C.-C. Tsai, W.-P. Hu and C. C. Wang, *Phys. Chem. Chem. Phys.*, 2020, **22**, 6528–6537.
- 63 S. Inomata, *ACS Earth Space Chem.*, 2021, **5**, 1929–1933.
- 64 S. M. Aschmann, A. Reissell, R. Atkinson and J. Arey, *J. Geophys. Res.: Atmos.*, 1998, **103**, 25553–25561.
- 65 M. J. Frisch, G. W. Trucks, H. B. Schlegel, G. E. Scuseria, M. A. Robb, J. R. Cheeseman, G. Scalmani, V. Barone, B. Mennucci, G. A. Petersson, H. Nakatsuji, M. Caricato, X. Li, H. P. Hratchian, A. F. Izmaylov, J. Bloino, G. Zheng, J. L. Sonnenberg, M. Hada, M. Ehara, K. Toyota, R. Fukuda, J. Hasegawa, M. Ishida, T. Nakajima, Y. Honda, O. Kitao, H. Nakai, T. Vreven, J. A. Montgomery, J. E. Peralta, F. Ogliaro, M. Bearpark, J. J. Heyd, E. Brothers, K. N. Kudin, V. N. Staroverov, R. Kobayashi, J. Normand, K. Raghavachari, A. Rendell, J. C. Burant, S. S. Iyengar, J. Tomasi, M. Cossi, N. Rega, J. M. Millam, M. Klene, J. E. Knox, J. B. Cross, V. Bakken, C. Adamo, J. Jaramillo, R. Gomperts, R. E. Stratmann, O. Yazyev, A. J. Austin, R. Cammi, C. Pomelli, J. W. Ochterski, R. L. Martin, K. Morokuma, V. G. Zakrzewski, G. A. Voth, P. Salvador, J. J. Dannenberg, S. Dapprich, A. D. Daniels, O. Farkas, J. B. Foresman, J. V. Ortiz, J. Cioslowski and D. J. Fox, *Gaussian 09, Revision A.02*, 2009.
- 66 K. Kristensen, L. N. Jensen, M. Glasius and M. Bilde, *Environ. Sci.: Processes Impacts*, 2017, **19**, 1220–1234.